Title:	Performance Evaluation of Active Islanding Detection Algorithms in Distributed Generation Photovoltaic Systems: Two Inverters Case
Authors:	E. J. Estébanez, V. M. Moreno, *IEEE, Member,* A. Pigazo, *IEEE, Member,* M. Liserre, *IEEE, Senior Member* and A. Dell'Aquila, *IEEE, Member*
Publication:	IEEE Transactions on Industrial Electronics, vol. 58, no. 4. April 2011. pp. 1185-1193.
D.O.I.:	10.1109/TIE.2010.2044132

Performance Evaluation of Active Islanding Detection Algorithms in Distributed Generation Photovoltaic Systems: Two Inverters Case

E. J. Estébanez, V. M. Moreno, *IEEE, Member,* A. Pigazo, *IEEE, Member,*
M. Liserre, *IEEE, Senior Member* and A. Dell'Aquila, *IEEE, Member*

***Abstract*—Grid-connected photovoltaic (PV) inverters employ an islanding detection functionality in order to determine the status of the electrical grid. In fact the inverter must be stopped once the islanding operation mode is detected according to the standards and grid-code limits.**

Diverse islanding detection algorithms have been proposed in literature to cope with this safety requirement. Among them active methods, based on the deliberate perturbation of the inverter behavior, can minimize the so called non detection zone (NDZ) that is the range of conditions in which the inverter does not recognize that is operating in undesired island. In most cases, the performances of these methods have been analyzed considering an highly dispersed generation scheme, where only one distributed generation power system (DGPS) is connected to the local electrical power system (EPS). However in some studies it has been highlighted that if two or more PV inverters are connected to the same local EPS, their anti-islanding algorithms do not behave ideally and can fail in detecting the islanding condition. However there is no systematic study that has investigated the overall capability of different anti-islanding methods employed on several inverters connected to the same EPS to detect islanding condition. This paper is a first attempt to carry out a systematic study of the performances of the most common active detection methods in case of two inverters connected to the same EPS. In order to evaluate the global capability of the two systems to detect islanding condition a new performance index is introduced and applied also to the case when the two inverters employ different anti-islanding algorithms.

I. Introduction

The number of DGPS in electrical systems have increased during the last decade due international policies about renewable energy sources and, in case of residential environments, the incomes due to DGPS have stimulated the interest of potential owners [1]-[5]. Most of these low-power and maintenance-free DGPS consist of one or two power electronic converters which ensure a maximum extraction of the available power and the proper current injection through an active front-end at the point of common coupling (PCC) of the DGPS, the local loads and the electrical grid. Such low-cost DGPS have a reduced number of sensors [6] and, in most cases, communication subsystems are not included, which would increase the complexity of grid management tasks [7].

E. J. Estébanez, V. M. Moreno and A. Pigazo are with the Dept. of Electronics and Computers, University of Cantabria, Santander, 39004 Spain (phone:+34-942-201338; fax: +34-942-201303; emails: estebanezej@unican.es, morenov@unican.es, pigazoa@unican.es).

M. Liserre and A. Dell'Aquila are with the Dep. of Electrical and Electronics Engineering, Polytechnic of Bari, Bari, 70126 Italy (emails: liserre@ieee.org, dellaqui@poliba.it).

This is the case of anti-islanding protections in grid-connected low-cost PV systems which, according to international standards [8]-[14], must be included in the DGPS active front-end in order to guarantee the safety of workers during maintenance operations of the electrical grid [15]. Moreover, this protection would avoid local loads to be damaged due to voltage and/or frequency excursions during the islanding condition and would protect the DGPS active front-end during the electrical grid reconnection. The detection of the islanding condition, defined in [8] as *a portion of the utility system that contains both load and distributed resources remains energized while it is isolated from the remainder of the utility system*, can be very difficult due to the electrical grid power system configuration and status while, according to [12], it must be detected and the inverter stopped within 2 s of the formation of the unintentional island.

Anti-islanding detection algorithms which reside in the controller of the inverter can be classified in passive and active methods [16]-[18]. Passive methods measure the voltage and current signals at the inverter side of the PCC in order to determine the islanding condition. This is the case of under/over voltage (OUV) and under/over frequency (OUF) methods [19][20] and methods based on the detection of the voltage/current harmonics [21][22] and phase variations [23][24]. The drawback of these methods is that it can not be guaranteed the detection of the islanding condition under all possible operation conditions [25]. In order to avoid this fact, active methods introduce a controlled disturbance at the PCC and, when the islanding condition occurs, the disturbance forces the detection method threshold [26][27]. The Active Frequency Drift (AFD) [28][29], the Sandia Frequency Shift (SFS) [30], the Slip Mode Frequency Shift (SMS) [21] and active/reactive power variation [31][32] methods are examples of such approach. The main drawbacks of these methods are that the injected disturbances can reduce the electrical power quality at the PCC and the fact they increase the complexity of the controller employed in the PV inverter.

In most cases, these methods have been proposed and analyzed considering a highly dispersed generation scheme, where the interaction between PV inverters can be avoided, but new policies and regulations about integration of PV systems in buildings [33]-[36] are changing this scenario, resulting on an higher number of low-power low-cost PV inverters connected to the same local EPS. As a result, some recent works have analyzed the interaction of certain active detection methods

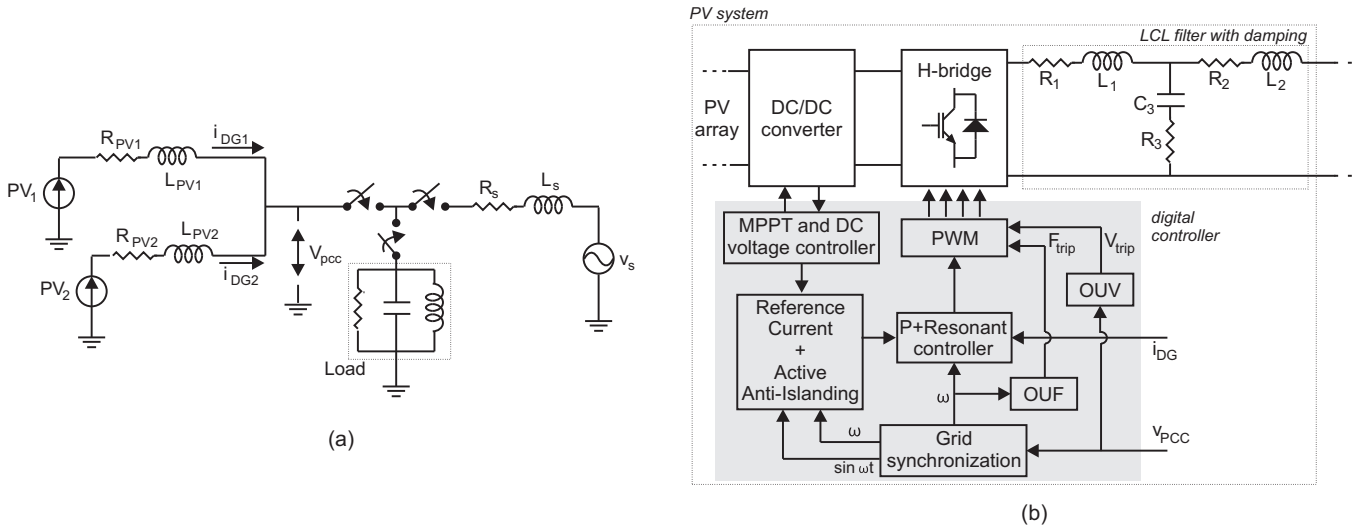

Fig. 1. General structure of a) the analyzed two-inverter configuration and b) each PV system. Parameters: $R_1 = 0.4\ \Omega$, $L_1 = 2$ mH, $R_2 = 0.3\ \Omega$, $L_2 = 1$ mH, $C_3 = 7\ \mu F$, $R_3 = 5.2\ \Omega$, $R_{load} = 52.9\ \Omega$, $C_{load} = 60.2\ \mu F$, $L = 168.4$ mH, $R_s = 0.8\ \Omega$, $L_s = 0.5$ mH, $f_{\rm pwm} = 6400$ Hz, $V_{dc} = 500$ V, $K_{\rm p,PLL} = 460$, $K_{\rm i,PLL} = 4.35 \cdot 10^{-3}$

under diverse operation conditions. The two inverters case has been analyzed considering the AFD method, in [37], SMS and Classical Linear Instability (CLI) methods, in [38], and SMS and positive AFD methods, in [39]. The multiple inverters case has been studied for active/reactive power variations, in [32], and SFS methods, in [40]. However there are no systematic studies that evaluate the islanding detection capabilities of different inverters employing different algorithms. The paper is a first attempt to fill this gap.

This paper evaluates the performance of the most common active islanding detection algorithms (AFD, SFS and SMS) considering the interaction between two PV inverters under the same comparison frame. The size of the Non-Detection Zone (NDZ) has been determined in each case in order to evaluate the obtained results.

II. Analyzed anti-islanding algorithms

The structure of the analyzed two DGPS topology is shown in Fig. 1.a, where two independent PV systems are considered and the grid-side impedance of each inverter can be changed in order to analyze diverse operation conditions in both residential and industrial EPS. Due to the employed active front-ends, the DGPS can be considered as current sources whose magnitudes, $\mid i_{DG1} \mid$ and $\mid i_{DG2} \mid$, depend on the solar irradiance. Three switches connected to the PCC allow islanding tests to be carried out according to IEEE Std. 1547.1 [13]. A test resonant load ($R_{\rm load}$, $C_{\rm load}$ and $L_{\rm load}$) with quality factor 1 has been considered during the islanding tests. The equivalent impedance of the PV inverters, considering the output LCL filter and the transformer, is denoted in Fig. 1.a by $R_{\rm PV}$ and $L_{\rm PV}$ while the impedance of the electrical grid at the point of common coupling is modeled by means of R_s and L_s. The measured voltage at the point of common coupling, $v_{\rm pcc}$, depends on the grid voltage while the electrical grid is connected. Once the islanding condition is applied, the PCC voltage depends only on the connected PV inverters.

The inner structure of each PV system is shown in Fig. 1.b. The DC/DC stage is operated using a Perturb & Observe (P&O) algorithm [41] that adapts the voltage of the PV array in order to track the maximum power point (MPP), as temperature and irradiation change, and keep constant the dc voltage at the input of the H-bridge full-bridge [42]. The P&O MPP controller increases or decreases the PV string voltage depending on the measured output power. If there is no output power variation, it maintains the converter duty cycle but, in case of power variation, and depending on the power and voltage slope, it increases or decreases the pv string voltage in order to find the MPP. The dc voltage, at the inverter side, is regulated by adjusting the current demand of the PV inverter depending on available solar irradiation. The controller establishes the switching states of the grid-connected current-controlled single-phase inverter through a pulse width modulator. Sideband harmonics of the modulator carrier signal are minimized by introducing a LCL filtering stage (R_1, L_1, R_2, L_2 and C_3) properly designed with damping resistor R_3 [43]. Other functional blocks inside the digital controller of the PV inverter are the grid synchronization, the generation of the reference signal for current injection purposes (including the evaluation of the current components which allow the active anti-islanding methods to be implemented), the current controller and the measurement of grid voltage and frequency for islanding detection. The PV inverter is synchronized to the electrical grid by means of a software phase locked loop (PLL) which takes advantage of the Park transformation in order to measure the electrical grid frequency, ω, and generate a pure sinusoidal signal in phase with the electrical grid, $\sin \omega t$. The behavior of this software PLL depends on the characteristics of the inner PI controller (settling time and ξ). More details about synchronization in grid connected inverters can be found in [44]. From $\sin \omega t$, ω and the MPPT controller output (the available solar power), the *Reference Current* block generates the reference signal for

power injection purposes. Its amplitude depends on the MPPT controller output while its phase is generated from $\sin \omega t$. This block also implements the generation of the controlled disturbance which must be injected at the PCC in order to reveal the islanding condition. The instantaneous values of the reference signal and the grid frequency measured by means of the PLL are applied to the current controller, which is made by one proportional component and several (the precise number of the required resonant blocks depends on the PCC voltage spectrum) resonant terms at the grid frequency. Depending on the measured grid frequency ω, the resonance frequency of the resonant term is changed. The impact of each resonant and the proportional blocks of the current controller is determined by means of gains, K_i and K_p respectively, whose value is determined depending on the PCC conditions (i.e. trying to avoid system instabilities). Details about the design process of this kind of controllers can be found in [45] and [46]. The grid rms voltage and frequency are measured in order to determine the islanding condition by means of Over-Under Voltage (OUV) and Over-Under Frequency (OUF) blocks. If this is the case, tripping signals V_{trip} and F_{trip} would stop the PV inverter.

The power balance between the two DGPS, the load and the grid in a system such as the one shown in Fig. 1.a is

$$P_{\text{load}} = P_{DG1} + P_{DG2} + \Delta P \quad (1)$$
$$Q_{\text{load}} = Q_{DG1} + Q_{DG2} + \Delta Q \quad (2)$$

where ΔP and ΔQ are the active and reactive powers supplied by the electrical grid to the local EPS and it has been considered negligible power losses associated to the inverter side impedances, P is the active power and Q the reactive power. P_{load} and Q_{load}, with a parallel RLC load (such as the test load from the IEEE Std. 1547.1), are defined as

$$P_{\text{load}} = V_{pcc}^2 \cdot R_{\text{load}}^{-1} \quad (3)$$
$$Q_{\text{load}} = V_{pcc}^2 \cdot [(\omega L_{\text{load}})^{-1} - \omega C_{\text{load}}]. \quad (4)$$

After the grid disconnection, the power of the load will be forced to be the same of the PV systems, therefore if ΔP was nonzero, it can be seen from (3) that the voltage at the PCC will increase or decrease until $P_{\text{load}} = P_{DG1} + P_{DG2}$. Similarly, if ΔQ was nonzero, the frequency and/or voltage will vary until $Q_{\text{load}} = Q_{DG1} + Q_{DG2}$ according to (4).

If ΔP and/or ΔQ are small, the voltage and/or frequency variation won't be enough to trigger the OUV/OUF blocks, and the islanding condition won't be detected. Since the probability of the islanding condition not being detected with this method is significant, active islanding detection methods, such as those described in the following sections, were developed in order to drift the voltage and/or frequency out of the boundaries with much lower power mismatch.

The following subsections describe the analyzed active anti-islanding methods: the Active Frequency Drift (AFD), Sandia Frequency Shift (SFS) and Slip Mode Frequency Shift (SMS) islanding detection methods.

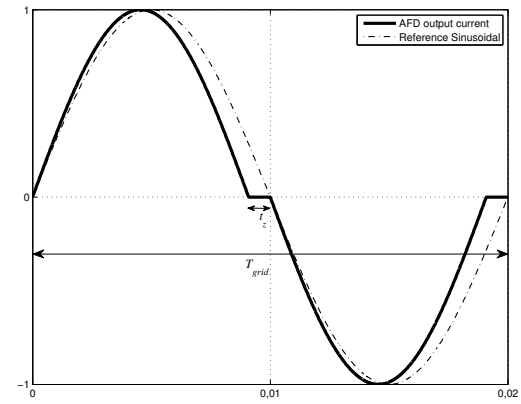

Fig. 2. AFD output current waveform.

A. Active Frequency Drift (AFD)

The Active Frequency Drift (AFD) method slightly alters the DGPS's output current waveform. One example of such an output current is shown in Fig. 2, along with a pure sinusoidal for comparison purposes. During the first portion of the first half-cycle, the output current is a sinusoid with a slightly higher frequency than the nominal. The difference between the nominal frequency of the electrical grid and the frequency of the output current is defined as Δf. When the current reach to zero, it remains that way for t_z s until the second half-cycle begins. For the first part of the second half-cycle, the output current is the negative of the first half-cycle, and when the current reaches zero for the second time, it remains that way until another cycle begins. The chopping factor is defined as

$$cf = \frac{t_z}{(T_{grid}/2)} \quad (5)$$

where t_z is the dead time and T_{grid} is the period of the grid voltage.

When the utility is present, it maintains the voltage frequency, but when it is absent, the frequency of the PCC voltage is determined by the current injected by the PV inverter and, hence, it tends to drift away from the nominal frequency of the grid until the island condition is detected by the OUF relays.

B. Sandia Frequency Shift (SFS)

The Sandia Frequency Shift (SFS) improves the performance of the AFD method by adding positive feedback to the AFD method in order to drift the frequency away from the nominal value faster than the classical method, and thus, the NDZ of the SFS is significantly reduced with respect to that of the AFD method. The chopping factor is varied according to the measured frequency drift:

$$cf_k = cf_0 + K(f_{k-1} - f_0) \quad (6)$$

where cf_0 is the initial chopping-factor, f_{k-1} the frequency of the grid voltage measured at the PCC at cycle $k-1$, f_0 the nominal grid frequency (50 Hz) and K is a positive feedback gain which allows the detection time of the islanding condition to be adjusted.

C. Slip Mode Frequency Shift (SMS)

The Slip Mode Frequency Shift (SMS) changes the phase angle of the PV inverter current $\theta_{SMS,k}$ according to the variation of the measured voltage frequency with respect to the nominal frequency of the electrical grid.

$$\theta_{\mathrm{SMS,k}} = \theta_m sin\left(\frac{\pi}{2}\frac{f_{k-1}-f_0}{f_m-f_0}\right), \tag{7}$$

where f_m is the frequency at which the maximum phase shift θ_m occurs. Usually, $f_m - f_0$ is taken as 3 Hz.

For example, if the frequency of the PCC voltage is slightly increased after the grid disconnection, the phase angle of the current is increased, which reduces the time to the next zero crossing of the PCC voltage. This is interpreted by the controller as a frequency increase, so the phase angle of the current is increased again, and so on, until the frequency surpasses the over frequency relay. Similarly, when the frequency of the PCC voltage decreases after the grid disconnection, the frequency is continuously decreased until it is detected by the under frequency relay.

D. Relative NDZ change

In order to compare the performance of the evaluated active anti-islanding methods and the effect of interaction in case of two PV inverters connected to the same EPS, the size of the NDZ has been evaluated from the obtained measurements. In this sense, it must be considered that the results of the islanding tests are shown in the load resonant frequency-quality factor space ($f - Q_f$) [29]. The size of the NDZ, considering a number of analysis points in the $f - Q_f$ space, can be evaluated by means of Riemann Sums as

$$S = \sum_{i\in \mathrm{NDZ}} \left(\frac{u_{i+1}+u_i}{2} - \frac{l_{i+1}+l_i}{2}\right)\cdot(\log q_{i+1} - \log q_i) \tag{8}$$

where index i allows all the obtained points in the NDZ to be computed, u and l are, respectively, the upper and lower bounding functions of the NDZ and q is a function which contains the load quality factor values. The values of S for a certain anti-islanding method i, S_i, are determined according to (8) and the accuracy of the obtained results depend on the employed simulation steps during the islanding test.

Considering that the tests are carried out using two inverters and all possible combinations of the analyzed active islanding detection methods, the relative change of the NDZ has been defined as

$$\Delta S_i = \frac{S_i - S_j}{S_j}\cdot 100[\%]. \tag{9}$$

where i corresponds to a certain analyzed anti-islanding method during the tests and j is the selected reference method for comparison purposes.

III. Simulation results

Simulation tests have been carried out using a model developed in MATLAB/Simulink according to the schema shown in Fig. 1. The NDZ has been evaluated in each case considering 0.9 to 1.1 $p.u.$ and 49 to 51 Hz as limits for OUV/OUF blocks. The simulation steps have been selected as 0.1 Hz for f_0 and 0.05 for $\log Q_f$ (due to employed logarithmic scale). The employed current controller considers four resonant blocks at fundamental, 3^{rd}, 5^{th} and 7^{th} harmonics and gains equal to $K_1 = K_3 = K_5 = K_7 = 1000$. The gain of the proportional block has been established at 7. The software PLL has been implemented in dq coordinates by means of a variable transport delay block which allows to generate the required q component properly. The inner PI controller of the PLL has been adjusted to operate with $\xi = 0.707$ and 0.02 s as settling time. The test load, as defined in IEEE Std. 1547.1, is a resonant parallel RLC load. The active and reactive powers injected by each PV inverter have been established at 1000 W and 0 VA respectively. The simulation analysis has been carried out considering the common operation conditions of each method. In case of AFD, negative and positive frequency variations have been analyzed with Δf equal to 0.5 and 1 Hz. Both signs of the chopping factor in the SFS method have been considered for accelerating gains equal to 0.05 and 0.1 Hz^{-1}. In case of SMS method, two values of θ_m have been considered ($10°$ and $15°$). The obtained results are shown in the following subsections.

A. Methods maintaining the NDZ

Certain combinations of the analyzed islanding detection methods will result on NDZs equal to the NDZ for one PV inverter, this is the case of both inverters running AFD with equal sign of Δf, two SFS with equal sign of cf_0 or two SMS. The obtained results, shown in Fig. 3.a and Fig. 3.b, have been evaluated by means of relative NDZs, according to (9), and considering the SMS method for $\theta_m = 10°$ as reference. The obtained results are shown in Table I. The worst results are obtained for AFD with equal sign of Δf, with a low influence of $\mid \Delta f \mid$ on the NDZ area (only 1.9%) but with a band shifting towards low frequencies at low load quality factors due to a higher $\mid \Delta f \mid$. From Fig. 3, and in case of $Q_f = 1$ and 50Hz resonance frequency, the AFD method with the employed software PLL and current controller would fail in the detection of the islanding condition. In case of $\Delta f = 1$Hz, the detection could be done by changing the PLL parameters. In case of the SFS method with equal signs of the initial chopping factors, doubling the value of K, from 0.05 Hz^{-1} to 0.1 Hz^{-1}, the size of the NDZ will decrease and its center will be shifted to higher values of the load quality factor (According to Fig. 3.b and using $K = 0.1$ Hz^{-1} the islanding tests with $Q_f < 35.5$ will be detected). As in case of the AFD method, the NDZ limits of the SFS method would change a bit depending on the characteristics of the employed PV inverter controllers (PLL, current controller, sampling frequency...). The results are improved by applying the SMS method to both inverters, obtaining the best ones at greater values of θ_m, but it must be considered that increasing the value of θ_m would result on an

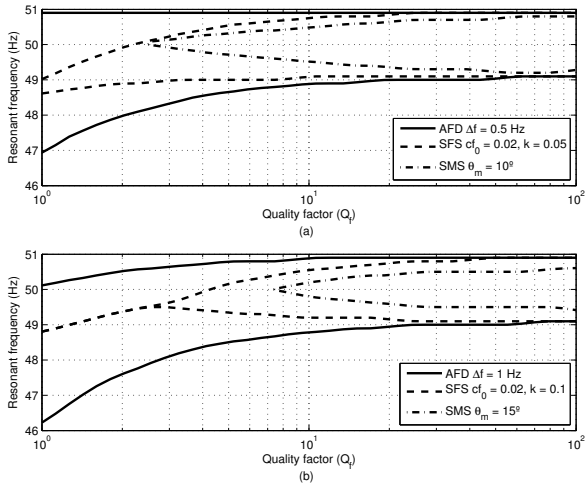

Fig. 3. NDZ of the analyzed AFD, SFS and SMS methods, matching the case with one inverter, for different parameters.

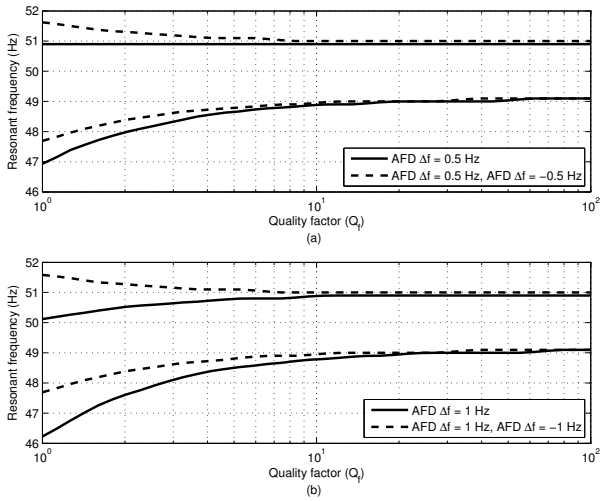

Fig. 4. NDZ of the two-inverters case with AFD and different signs of Δf compared to two inverters and positive Δf. a) $\mid \Delta f \mid = 0.5$ Hz and b) $\mid \Delta f \mid = 1$ Hz.

TABLE I
RELATIVE SIZE OF THE NDZS IN CASE OF NO VARIATION FROM THE ONE INVERTER CASE. $S_j = 1.72$.

AFD $\Delta f = 0.5$ Hz	$+165.8\%$
AFD $\Delta f = 1$ Hz	$+167.7\%$
SFS $cf = 0.02$ $K = 0.05$ Hz^{-1}	$+74.1\%$
SFS $cf = 0.02$ $K = 0.1$ Hz^{-1}	$+22.2\%$
SMS $\theta_m = 15^\circ$	-46.2%

higher system instability which could cause a false trip during normal operation.

B. Methods resulting on a worst NDZ

This subsection summarizes the results for the two PV inverters case when the obtained NDZs become worst. The results are grouped in five figures corresponding to interactions between AFD methods, SFS methods and interactions

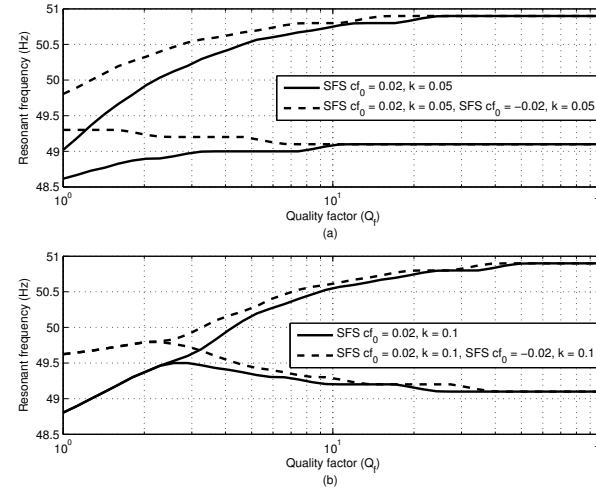

Fig. 5. NDZ of two PV inverter with the SFS method considering different signs of cf_0 and compared to the case of equal signs. a) $K = 0.05$ and b) $K = 0.1$.

TABLE II
RELATIVE SIZE OF THE NDZS IN CASE OF AFD METHODS WITH DIFFERENT SIGN. $S_j = 4.56$.

AFD $\Delta f = \pm 0.5$ Hz	$+1.8\%$
AFD $\Delta f = \pm 1$ Hz	$+1.2\%$
AFD $\Delta f = +1$ Hz	$+0.7\%$

TABLE III
RELATIVE SIZE OF THE NDZS IN CASE OF TWO INVERTERS WITH SFS METHODS AND DIFFERENT SIGN IN cf_0. $S_j = 2.10$.

SFS $cf_0 = \pm 0.02$, $K = 0.05$	$+45.5\%$
SFS $cf_0 = +0.02$, $K = 0.05$	$+42.5\%$
SFS $cf_0 = \pm 0.02$, $K = 0.1$	$+1.8\%$

considering crossing methods (SFS+AFD, SMS+AFD and SMS+SFS).

The effect of frequency drift with different sign when the AFD method is implemented in both PV inverters is shown in Fig. 4. The obtained relative NDZs, considering the method with $\Delta f = +0.5\ Hz$ as reference, are shown in Table II. As it can be seen, increasing the magnitude of the frequency variation, and maintaining opposite signs in each PV inverters, will result on a bit smaller NDZ (from $\mid \Delta f \mid = 0.5$Hz to $\mid \Delta f \mid = 1$Hz the relative size decreases only 0.6%) but greater than the obtained one in case of equal signs. From Fig. 4.b, changing the control parameters of the PV inverter would be not sufficient to detect the islanding condition at $Q_f = 1.0$ and 50 Hz resonant frequency and, hence, would fail passing the islanding tests in the international standards.

The interaction of SFS methods in case of cf_0 with different signs is presented in Fig. 5, where, in each subfigure, it is compared to the case with two inverters and equal sign. The relative sizes of the NDZs, considering SFS $cf_0 = +0.02$ $K = 0.1$ in both inverters as a reference, are given in Table III. As it can be seen, applying opposite signs to the initial chopping factor would result on a NDZ which is deformed towards low load resonance frequencies at low quality factors. Moreover,

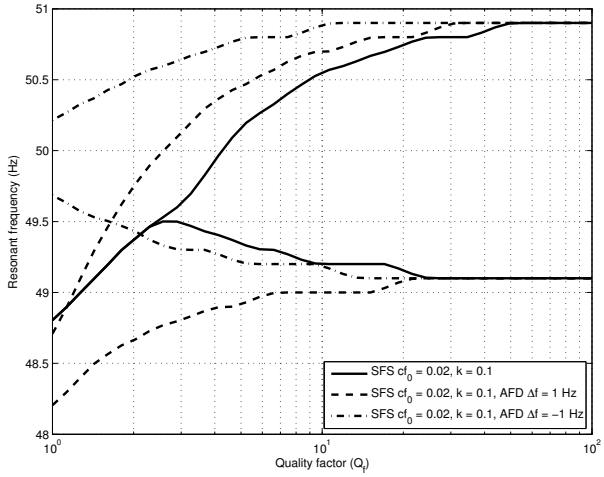

Fig. 6. NDZs due to the interaction of SFS and AFD methods.

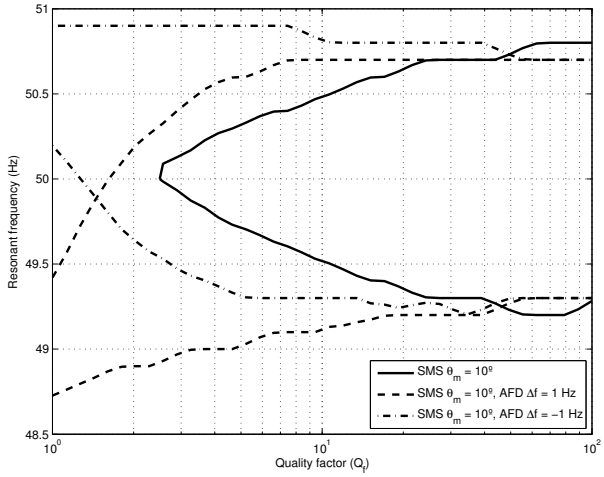

Fig. 7. NDZs due to the interaction of SMS and AFD methods.

TABLE IV
RELATIVE SIZE OF THE NDZS IN CASE OF TWO INVERTERS WITH SFS AND AFD METHODS. $S_j = 2.10$.

SFS $cf_0 = 0.02$, $K = 0.1$ and AFD $\Delta f = +1$ Hz	$+44.3\%$
SFS $cf_0 = 0.02$, $K = 0.1$ and AFD $\Delta f = -1$ Hz	$+46.0\%$

at a certain value of K, applying equal initial chopping factors with opposite sign will result on a higher NDZ in comparison to the equal signs case (the NDZ increases 1.8% at $K = 0.1$ and 2.2% at $K = 0.05$). From an islanding test compliance point of view, in case of lower K values, the upper bound of the NDZ approaches the most to 50 Hz. This could cause the PV inverter controllers, under certain implementations, to fail in the detection of the islanding condition. In fact, at 50 Hz, the upper bound of the NDZ of the two inverters case with oposite cf_0, in Fig. 5 is reached at $Q_f = 2.0$.

The effect of two different active strategies for detection of the islanding condition has been also evaluated. Fig. 6 compares the NDZs of two PV inverters running SFS and AFD islanding detection algorithms. As it can be seen, the

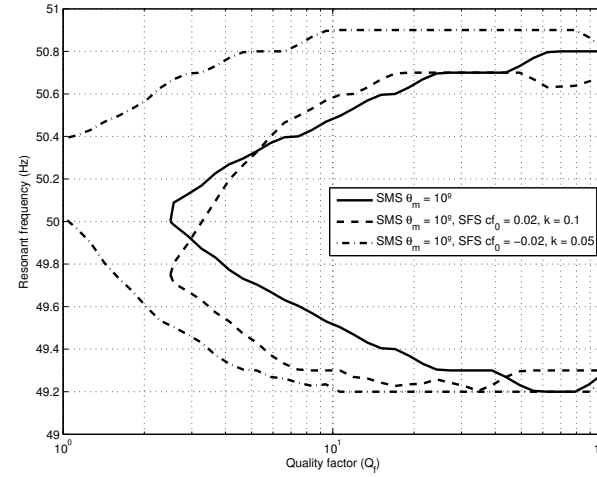

Fig. 8. NDZs due to the interaction of SMS and SFS methods.

TABLE V
RELATIVE SIZE OF THE NDZS IN CASE OF TWO INVERTERS WITH SMS AND AFD METHODS. $S_j = 1.72$.

SMS $\theta_m = 10^\circ$ and AFD $\Delta f = +1$ Hz	$+65.4\%$
SMS $\theta_m = 10^\circ$ and AFD $\Delta f = -1$ Hz	$+65.4\%$

initial NDZ, which corresponds to the case of two inverters running SFS with $cf_0 = 0.02$ and $K = 0.1$ will be increased at lower values of Q_f by changing the detection algorithm in one of the PV inverters and applying the AFD method with $\Delta f = +1$ Hz. The effect is higher in case of the AFD method with negative Δf, where the NDZ size increases and the aspect changes, reaching higher values of f_0 at lower Q_f. Considering test conditions at 50 Hz and $Q_f = 1$, the AFD method with negative Δf would cause both inverters, operating simultaneously, to fail the detection of the islanding condition. Table IV shows the relative sizes of the NDZs considering the SFS method, with $cf_0 = 0.02$ and $K = 0.1$, as reference.

The effect of the interaction of the SMS and AFD detection methods is shown in Fig. 7. As it can be seen, the NDZ corresponding to two SMS algorithms with $\theta_m = 10^\circ$ will increase when applying the AFD method in one of the PV inverters. Depending on the sign of Δf, the upper and lower bounds of the NDZ will fall at low Q_f (positive Δf) or increase (negative Δf). In case of negative Δf, the resulting lower bound of the NDZ crosses the $50\ Hz$ value at $Q_f = 2.2$ while, for positive Δf, the value of Q_f at 50 Hz is a bit better ($Q_f = 6.8$). The relative values of the NDZs are shown in Table V, where the SMS method with $\theta_m = 10^\circ$ has been considered as reference. The relative size of the obtained NDZs is the same due to the fact that there is no a predefined frequency drift sense in the SMS method.

The impact of the SFS method on the NDZ of the SMS method is depicted in Fig. 8. The aspect change of the NDZ due to the SFS method is higher in case of lower values of K. As in case of SMS and AFD methods, the effect of the sign associated to cf_0 can be neglected when evaluating the

TABLE VII
IMPACT OF ACTIVE ANTI-ISLANDING ALGORITHMS IN CASE OF TWO INVERTERS.

PV_1 \ PV_2	SMS	SFS	AFD
SMS	[0.9,1.7]	-	-
SFS	$+76.9\%$ / -11.5%	[2.1,3.0]	-
AFD	$+161.5\%$ / -26.1%	$+7.7\%$ / -39.1%	[4.5,4.6]

TABLE VI
RELATIVE SIZE OF THE NDZS IN CASE OF TWO INVERTERS WITH SMS AND SFS METHODS. $S_j = 1.72$.

SMS $\theta_m = 10^\circ$ and SFS $cf_0 = +0.02$, $K = 0.1$	$+9.8\%$
SMS $\theta_m = 10^\circ$ and SFS $cf_0 = -0.02$, $K = 0.05$	$+57.1\%$

size of the NDZ. The relative size of the obtained NDZs is compared in Table VI, where the SMS method with $\theta_m = 10^\circ$ has been considered as reference. From Fig. 8 the SFS method with positive chopping factor cause the initial NDZ to be shifted towards lower resonant frequencies while negative chopping factors increase the NDZ size and could cause the non-detection of the islanding condition around $50\ Hz$ and $Q_f = 1$.

IV. DISCUSSION

The obtained simulation results are summarized in Table VII. The configuration parameters of each analyzed active anti-islanding method have been varied inside the recommended ranges in literature and, in case of both methods corresponding to the same family, the obtained sizes S_i for the NDZs are shown as a range, which has been obtained during the tests by applying (8). From these ranges, the smallest range corresponds to the case of two PV inverters running SMS methods while the worst one is obtained in case of two AFD algorithms. From a practical point of view, issues such as the output current THD, complexity of the controller or the inverter stability should be also considered.

The impact of two different detection algorithms on the NDZs is shown by means of relative NDZs which have been obtained considering the midpoints of the obtained ranges for the NDZ sizes. The upper percentage in each cell has been evaluated considering the method running in the second PV inverter as a reference while the low one employs the method in PV_1 as reference. As it can be seen, the initial size range for the SMS methods will get worst by changing one of the SMS to SFS, which, in average, will result on a $+76.9\%$ greater NDZ. In case of AFD, the obtained results are the worst ones and the NDZ which will increase up to $+161.5\%$. In case of two inverters running the SFS methods initially, changing one of the inverters by a new one including SMS would reduce the resulting NDZ in a 11.5% while employing the AFD algorithm would increase it, in average, up to 7.7%. Finally, if two AFD algorithms are running initially, the resulting NDZ can be improved by changing one of the inverters to SMS or SFS, obtaining the best results in case of the SFS, which would allow the initial NDZ to be reduced up to -39.1%.

V. CONCLUSION

This article analyzes the performance of the most common active islanding detection algorithms in case of two PV inverters connected to the same EPS. The analyzed methods are Active Frequency Drift (AFD), Sandia Frequency Shift (SFS) and Slip Mode Frequency Shift (SMS). Once the islanding detection methods are described, a new index which allows the comparison of the obtained non-detection zones is defined. This index, the relative size of the NDZs, is employed in order to evaluate the overall capability to detect the island operation in case different inverters employs different algorithms. Finally, considering two PV inverters running the same family of islanding detection methods, the best option for change one of the inverter algorithm, in order to reduce the NDZ, is given. From the obtained results, the best NDZ is obtained when both inverters executes the SMS algorithm. In case of two different inverters, and one of them running SFS, the other one should execute SMS in order to minimize the NDZ. In case of AFD, it is recommended to employ a second inverter implementing a SFS method. These indications can be sued as a guideline when installing new inverters in a EPS where others are already connected.

ACKNOWLEDGMENT

The work in this paper was supported by the Spanish Ministry of Science and Innovation under grant ENE2007-63979/ALT.

REFERENCES

[1] F. Blaabjerg, R. Teodorescu, Z. Chen and M. Liserre, "Power Converters and Control of Renewable Energy Systems," in *Proc. of ICPE 2004,* Pusan, Korea, October 2004. Invited paper.

[2] J. M. Carrasco, L. G. Franquelo, J. T. Bialasiewicz, E. Galvn, R. C. P. Guisado, M. M. Prats, J. I. Len and N. Moreno-Alfonso, "Power electronic systems for the grid integration of renewable energy sources: A survey," *IEEE Transactions on Industrial Electronics,* vol. 53, no. 4, August 2006. pp. 1002-1016.

[3] F. Blaabjerg, R. Teodorescu, M. Liserre and A. V. Timbus, "Overview of control and grid synchronization for distributed power systems," *IEEE Transactions on Industrial Electronics,* vol. 53, no. 5, October 2006. pp. 1398-1409.

[4] F. Blaabjerg, Z. Chen and S. B. Kjaer, "Power electronics as efficient interface in dispersed power generation systems," *IEEE Transactions on Power Electronics*, vol. 19, no. 5, Sept. 2004. pp. 1184-1194.

[5] J.-S. Lai, "Power conditioning circuit topologies," *IEEE Industrial Electronics Magazine,* vol. 3, no. 2, June 2009. pp. 24-34.

[6] M. E. Ropp, K. Aaker, J. Haigh and N. Sabbah, "Using power line carrier communications to prevent islanding [of PV power systems]," *in Proc. of the* 28^{th} *IEEE Photovoltaic Spec. Conf.,* September 2000. pp. 1675-1678.

[7] P. L. Villeneuve, "Concerns generated by islanding," *IEEE Power & Energy Magazine,* vol. 2, no. 3, May/June 2004. pp. 49-53.

[8] *IEEE Recommended Practice for Utility Interface of Photovoltaic (PV) Systems,* IEEE Std. 929-2000. 2000.

[9] *Photovoltaic (PV) Systems - Characteristics of the utility interface,* IEC61727. 2004.

[10] *Testing procedure of islanding prevention measures for utility interactive photovoltaic inverters,* IEC 62116.

[11] *Automatic disconnection device between generator and the public low-voltage grid,* VDE0126-1-1. (IEC 82/429/CDV:2006), Deutsche Fassung prEN 62108:2006 (in German).

[12] *IEEE Standard for Interconnecting Distributed Resources with Electric Power Systems,* IEEE Std. 1547-2003, July 2003.

[13] *IEEE Standard Conformance Test Procedures for Equipment Interconnecting Distributed Resources with Electric Power Systems,* IEEE Std. 1547.1-2005, July 2005.

[14] *IEEE Draft Application Guide for IEEE Standard 1547, Interconnecting Distributed Resources with Electric Power Systems,* IEEE P1547.2/D10, March 2008.

[15] R. A. Walling and N. W. Miller, "Distributed generation islanding-implications on power system dynamic performance," in *Proc. of 2002 IEEE Power Engineering Society Summer Meeting,* vol. 1, July 2002. pp. 92-96.

[16] G. Petrone, G. Spagnuolo, R. Teodorescu, M. Veerachary and M. Vitelli, "Reliability Issues in Photovoltaic Power Processing Systems," *IEEE Transactions on Industrial Electronics,* vol. 55, no. 7, July 2008. pp.2569-2580.

[17] F. De Mango, M. Liserre and A. DellAquila, "Overview of anti-islanding algorithms for PV systems. Part II: active methods", in *Proc. of EPE-PEMC 2006,* Portoroz, Slovenia, August 2006. pp. 1884-1889.

[18] F. De Mango, M. Liserre, A. DellAquila and A. Pigazo, "Overview of anti-islanding algorithms for PV systems. Part I: passive methods", in *Proc. of EPE-PEMC 2006,* Portoroz, Slovenia, August 2006. pp. 1878-1883.

[19] S. Islam, A. Woyte, R. Belmans, P. Heskes, P. M. Rooij and R. Hogedoorn, "Cost effective second generation AC-modules: Development and testing aspects," *Energy,* vol. 31, no. 12, September 2006. pp. 1897-1920.

[20] J.-M. Kwon, K.-H. Nam and B.-H. Kwon, "Photovoltaic power conditioning system with line connection," *IEEE Transactions on Industrial Electronics,* vol. 53, no. 4, June 2006. pp. 1048-1054.

[21] W. Bower and M. Ropp, *Evaluation of islanding detection methods for photovoltaic utility-interactive power systems,* Tech. Rep. IEA-PVPS T5-09:2002, December 2002.

[22] A. Pigazo, M. Liserre, R. A. Mastromauro, V. M. Moreno and A. Dell'Aquila, "Wavelet-based Islanding Detection in Grid-Connected PV Systems," *IEEE Transactions on Industrial Electronics,* vol. 56, no. 11, November 2009. pp. 4445-4455.

[23] M. E. Ropp, M. Begovic, A. Rohatgi, G. A. Kern, R. H. Bonn, Sr., and S. Gonzalez, "Determining the relative effectiveness of islanding detection methods using phase criteria and nondetection zones," *IEEE Transactions on Energy Conversion,* vol. 15, no. 3, September 2000. pp. 290-296.

[24] K. El-Arroudi, G. Jos, I. Kamwa and D. T. McGillis, "Intelligentbased approach to islanding detection in distributed generation," *IEEE Transactions on Power Delivery,* vol. 22, no. 2, April 2007. pp. 828-835.

[25] M. Liserre, A. Pigazo, A. Dell'Aquila and V. M. Moreno, "An antiislanding method for single-phase inverters based on a grid voltage sensorless control," *IEEE Transactions on Industrial Electronics,* vol. 53, no. 5, October 2006. pp. 1418-1426.

[26] G.-K. Hung, C.-C. Chang and C.-L. Chen, "Automatic phase-shift method for islanding detection of grid-connected photovoltaic inverters," *IEEE Transactions on Energy Conversion,* vol. 18, no. 1, March 2003. pp. 169-173.

[27] J. B. Jeong and H. J. Kim, "Active anti-islanding method for PV system using reactive power control," *Electronics Letters,* vol. 42, no. 17, August 2006. pp. 1004-1005.

[28] M. E. Ropp, M. Begovic and A. Rohatgi, "Analysis and performance assessment of the active frequency drift method of islanding prevention," *IEEE Transactions on Energy conversion,* vol. 14, no. 3, September 1999. pp. 810-816.

[29] L. A. C. Lopes and H. Sun, "Performance assessment of active frequency drifting islanding detection methods," *IEEE Transactions on Energy Conversion,* vol. 21, no. 1, March 2006. pp. 171-180.

[30] H. H. Zeineldin and S. Kennedy, "Sandia Frequency-Shift Parameter Selection to Eliminate Nondetection Zones," *IEEE Transactions on Power Delivery,* vol. 24, no. 1, January 2009. pp. 486-487.

[31] C. Jeraputra and P. N. Enjeti, "Development of a Robust Anti-Islanding Algorithm for Utility Interconnection of Distributed Fuel Cell Powered Generation," *IEEE Transactions on Power Electronics,* vol. 19, no. 5, Sept. 2004. pp. 1163-1170.

[32] C. Jeraputra, E. C. Aeloiza, P. N. Enjeti and S. Choi, "An Improved Anti-Islanding Algorithm for Utility Interconnection of Multiple Distributed Fuel Cell Powered Generations," in *Proc. of the* 20^{th} *IEEE Applied Power Electronics Conference and Exposition,* vol. 1, March 2005. pp. 103-108.

[33] D. H. W. Li, T. N. T. Lam, W. W. H. Chan and A. H. L. Mak, "Energy and cost analysis of semi-transparent photovoltaic in office buildings," *Applied Energy,* vol. 86, no. 5, May 2009. pp. 722-729.

[34] L. Y. Seng, G. Lalchand and G. M. S. Lin, "Economical, environmental and technical analysis of building integrated photovoltaic systems in Malaysia," *Energy Policy,* vol. 36, no. 6, June 2008. pp. 2130-2142.

[35] A. Zahedi, "Solar photovoltaic (PV) energy; latest developments in the building integrated and hybrid PV systems," *Renewable Energy,* vol. 31, no. 5, April 2006. pp. 711-718.

[36] M. Ordenes, D. L. Marinoski, P. Braun and R. Rther, "The impact of building-integrated photovoltaics on the energy demand of multi-family dwellings in Brazil," *Energy and Buildings,* vol. 39, no. 6, June 2007. pp. 629-642.

[37] L. A. C. Lopes and Y. Zhang, "Islanding Detection Assessment of Multi-Inverter Systems With Active Frequency Drifting Methods," *IEEE Transactions on Power Delivery,* vol. 23, no. 1, January 2008. pp. 480-486.

[38] R. Bhandari, S. González and M. E. Ropp, "Investigation of Two Anti-Islanding Methods in the Multi-Inverter Case," *in Proc. of the IEEE Power and Engineering Society General Meeting - Conversion and Delivery of Electrical Energy in the* 21^{st} *Century,* July 2008. pp. 7.

[39] M. Xue, F. Liu, Y. Kang and Y. Zhang, "Investigation of active islanding detection methods in multiple grid-connected converters," in *Proc. of the IEEE* 6^{th} *International Power Electronics and Motion Control Conference,* May 2009. pp. 2151-2154.

[40] X. Wang, W. Freitas, V. Dinavahi and W. Xu, "Investigation of Positive Feedback Anti-Islanding Control for Multiple Inverter-Based Distributed Generators," *IEEE Transactions on Power Systems,* vol. 24, no. 2, May 2009. pp. 785-795.

[41] N. Femia, D. Granozio, G. Petrone, G. Spagnuolo and M. Vitelli, "Predictive & adaptative MPPT perturb and observe method," *IEEE Transactions on Aerospace and Electronic Systems,* vol. 43, no. 3, July 2007. pp. 934- 950.

[42] N. Femia, G. Lisi, G. Petrone, G. Spagnuolo and M. Vitelli, "Distributed Maximum Power Point Tracking of Photovoltaic Arrays: Novel Approach and System Analysis," *IEEE Transactions on Industrial Electronics,* vol. 55, no. 7, July 2008. pp. 2610-2621.

[43] M. Liserre, R. Teodorescu and F. Blaabjerg, "Stability of grid-connected PV inverters with large grid impedance variation," in *Proc. of IEEE* 35^{th} *Annual Power Electronics Specialist Conference,* vol. 6, June 2004. pp. 4773-4779.

[44] V. M. Moreno, M. Liserre, A. Pigazo and A. Dell'Aquila "A Comparative Analysis of Real-Time Algorithms for Power Signal Decomposition in Multiple Synchronous Reference Frames," *IEEE Transactions on Power Electronics,* vol. 22, no. 4, July 2007. pp. 1280-1289.

[45] R. Teodorescu, F. Blaabjerg, M. Liserre and P. C. Loh, "Proportional-resonant controllers and filters for grid-connected voltage-source converters," *IEE Proceedings-Electric Power Applications,* vol. 153, no. 5, Sept. 2006. pp. 750-762.

[46] A. V. Timbus, M. Ciobotaru, R. Teodorescu and F. Blaabjerg, "Adaptive resonant controller for grid-connected converters in distributed power generation systems," in *Proc. of the* 21^{st} *Annual IEEE Applied Power Electronics Conference and Exposition, 2006 (APEC'06),* March 2006. pp. 1601-1606.

Emilio J. Estébanez received the M.Sc. degree in telecommunications engineering (radiocommunications) from the University of Cantabria, Santander, Spain in 2007.

He is currently a Researcher on the Project ENE2007-63979/ALT "Islanding detection algorithms for low-voltage grid-connected inverters in photovoltaic distributed generation systems according to the EU standards (IDAPhoS)". His main research interests include electrical power quality and digital signal processing techniques applied to the control of power converters.

Víctor M. Moreno (M'01) received the M.Sc. and the Ph.D. degrees in physics (electronics) from the University of Cantabria, Santander, Spain, in 1980 and 1994 respectively.

He is currently an Associate Professor with the Department of Electronics and Computers, University of Cantabria. His research interests include electrical power quality, electromagnetic compatibility, digital signal processing and digital control of power converters.

Dr. Moreno is member of the IEEE Power Electronics Society (PELS). He was recipient of the Viesgo Award, in 1994, for his Ph.D. thesis, entitled *Distributed System for the Measurement and Analysis of Electrical Power Quality Applying Kalman Filtering*. He has been collaborating for IEEE journals as a Reviewer.

Alberto Pigazo (M'05) received the M.Sc. and the Ph.D. degrees in physics (electronics) from the University of Cantabria, Santander, Spain, in 1997 and 2004 respectively.

He was a Visiting Researcher and Professor with the Politecnico di Bari, Bari, Italy. Since October 2000, he has been with the Department of Electronics and Computers, University of Cantabria, where he is currently an Assistant Professor teaching courses in electronics, power electronics and digital signal processing. His main research interests include electrical power quality and digital signal processing techniques applied to the control of power converters.

Dr. Pigazo is member of the IEEE Industrial Electronics Society (IES), the Editorial Board of the IEEE INDUSTRIAL ELECTRONICS MAGAZINE and the IES Technical Committee on Renewable Energy Systems. As an author and Reviewer, he has been contributing for IEEE conferences and journals

Marco Liserre (S'00-M'02-SM'07) received the M.Sc. and Ph.D. degrees in electrical engineering from the Polytechnic of Bari, Bari, Italy, in 1998 and 2002, respectively.

Since January 2004, he has been an Assistant Professor with the Polytechnic of Bari, where he is engaged in teaching courses of power electronics, industrial electronics, and electrical machines. He has authored or coauthored more than 127 technical papers, 28 of them published or to be published in international peer-reviewed journals, and three chapters of a book. These works have received more than 800 citations.

He has been a visiting Professor at Aalborg University, Denmark, Alcala de Henares, Spain, and at Christian-Albrechts University of Kiel, Germany. He has been giving lectures in different universities and tutorials for the following conferences: IEEE Energy Conversion Congress and Exposition (ECCE) 2009, IEEE Power Electronics Specialists Conference (PESC) 2008, International Symposium on Industrial Electronics (ISIE) 2008, European Conference on Power Electronics and Applications (EPE) 2007, Annual Conference of the IEEE Industrial Electronics Society (IECON) 2006, ISIE 2006, and IECON 2005. His current research interests include industrial electronics applications to distributed power generation systems based on renewable energies.

Dr. Liserre is a senior member of the following societies: Industrial Electronics Society (IES), Power Electronics Society, Industry Applications Society and Power & Energy Society. He was a Reviewer for international conferences and journals. Within the IES, he has been responsible for student activities, an AdCom member, an Editor of the newsletter, and responsible for region 8 membership activities. He has been involved in the IEEE conferences organization in different capacities. He is an Associate Editor of the IEEE TRANSACTIONS ON INDUSTRIAL ELECTRONICS. He is the Founder and the Editor-in-Chief of the IEEE INDUSTRIAL ELECTRONICS MAGAZINE 2007-2009. He is Associate Editor of the new journal IEEE TRANSACTIONS ON SUSTAINABLE ENERGY starting in 2010. He is the Founder and the Chairman of the Technical Committee on Renewable Energy Systems of the IEEE Industrial Electronics Society. He has been a Guest Co-Editor-in-Chief of the IEEE TRANSACTIONS ON INDUSTRIAL ELECTRONICS for several Special Sections. He has received the IES 2009 Early Career Award. From 2010 he will be IEEE-IES Vice-President for publications.

Dr. Liserre will be the Co-Chairman of the International Symposium on Industrial Electronics (ISIE 2010), that will be held in Bari 4-7 July 2010.

Prof. Antonio Dell'Aquila (M'87) received the M.Sc. degree in Electrical Engineering from the Universit di Bari in 1970. Since 1970, he has been working with the Converters, Electrical Machines and Drives Research Team at the Universit di Bari. He is currently a Full Professor of Electrical Machines at the Politecnico di Bari, Italy, where he is also in charge of courses on power electronics and electrical drives. He has published over 100 technical papers in the fields of electrical machines models, transient analysis of rotating machines, inverter-fed induction machine performance, digital signal processing for non-sinusoidal waveforms, Kalman filtering for real-time estimation of induction motor parameters, control, monitoring and diagnostic of ac drives. His research current interests include harmonic pollution produced by electronic power systems, PWM techniques for power converters, power converters in renewable energy conversion systems, active power filters, multilevel inverters and intelligent control of power electronics equipment with fuzzy logic controllers.

Prof. A. Dell'Aquila is a member of the IEEE Power Engineering Society and of the Italian Electrotechnical and Electronic Association (A.E.I.). He is Dean of the Engineering Faculty of Politecnico di Bari.